International Journal of
Structural Engineering and Analysis
ISSN: 2456-5326
Vol. 6: Issue 2
www.journalspub.com

Finite Element Modeling of RC Beam Column Sub-assemblages Subjected to Column Loss Scenario

Sanjeev Bhatta[1,]* Jian Yang[2], Qing-Feng Liu[3]
[1]Master Student, School of Naval Architecture Ocean and Civil Engineering, Shanghai Jiao Tong University, Shanghai, China
[2]Professor, School of Naval Architecture, Ocean and Civil Engineering, Shanghai Jiao Tong University, China
[3]Associate Professor, School of Naval Architecture, Ocean and Civil Engineering, Shanghai Jiao Tong University, China

ABSTRACT

Progressive collapse is a situation where a failure of whole or large part of a structure occurs that has been initiated by failure of a relatively small part of the structure such as failure of any primary structural element. When a vertical load carrying element, typically a column is lost, the loads that are supposed to pass through lost column need to be safely transferred to the adjacent elements to prevent progressive collapse. This paper presents a computational investigation on failure modes and structural behavior of RC beam column sub-assemblages subjected to progressive collapse. For this purpose six finite element models are developed in ABAQUS, each comprising two span beams and three columns and the mechanism of progressive collapse resistance in middle column missing scenario is analyzed under mid span point loading in different stages of deflections. The finite element models are validated by comparing the results with the experimental results in literature. Good agreement is observed, which validates the capability of models to predict the structural behavior of RC beam column sub-assemblages in progressive collapse event with satisfactory accuracy, in spite of performing costly, time consuming non repeatable experimental works. Moreover, a parametric study is performed to examine the effects of beam top longitudinal rebar ratio, beam bottom longitudinal rebar ratio and beam span-to-height ratio on the global structural behavior of beam-column sub-assemblages. Structures with higher energy absorption capacity boost progressive collapse resistance mechanism. Hence energy absorption capacity of finite element models are compared and discussed.

Keywords: *Finite element, Beam-column sub-assemblage, Progressive collapse, Compressive arch action, Catenary action.*

****Corresponding Author***
E-mail: sanjeev.sapsan@gmail.com

INTRODUCTION

Research on progressive collapse of structures has intensified since the partial collapse of Ronan Point apartment building in London, UK in 1968. General Service Administration [1] defined progressive collapse as a situation where local failure of primary structural elements causes the collapse of adjacent structural elements which, in turn causes the collapse

of whole structure. It may be triggered by any intentional or unintentional action such as blast, vehicle impact, earthquake, and uncontrolled fire. In recent years, the engineering community has viewed with greater attention to the vulnerability of high rise buildings to progressive collapse, which could results substantial hazard to human life. To improve the performance of structure under such abnormal loading conditions, International Building Code [2] introduced provision of structural integrity requirements for design of multistory buildings. The American Concrete Institute Building code [3]requires a minimum level of structural integrity to be integrated in the structure to improve the structural performance in the event of column loss. Two well cited guidelines published by General Service Administration [1] and Department of Defense [4] provides necessary requirements for design of multistory buildings to prevent progressive collapse.

An increase in loss caused by progressive collapse events has led to the extension of research works concentrating on prediction of structural behavior. Four full-scale interior RC beam-column sub-assemblages were investigated by Qing and Li [5] with varying degree of non-seismic detailing after the RC moment resisting frame is subjected to the loss of its ground-story exterior column. Yap and Li [6] tested two series of specimens to investigate the performance of RC under exterior beam column sub-assemblages on loss of exterior ground column scenario. Six RC beam-column sub-assemblages were quasi statically tested by Yu and Tan [7] under a middle column removal scenario and suggested a deflection criterion to determine the capacity of RC sub-assemblages. Moreover, Alogla et al. [8] tested four specimens under quasi-static loading for a column loss scenario. In this study three specimens were provided with additional steel bars at the mid depth of the beam in order to optimize the best location for the added reinforcement bars. Experimental and numerical study performed by Rashidian et al. [9], considering the transverse beam, demonstrate a general enhancement on the capacity of specimens in the compressive arch action. Furthermore, Yu and Tan [10] carried out experimental study incorporating some special detailing techniques on reinforced concrete frame specimen to investigate the structural behavior under a column removal scenario. To obtain the better understanding of structural interactions among slabs, beams and columns, Lim et al. [11] tested 3D reinforced concrete substructures under different column removal position scenario. In-situ test of reinforced concrete building was carried out by Sasani et al. [12] to study the dynamic performance of the building subjected to sudden loss of exterior ground vertical structural element. Experimental study was conducted by Yi et al. [13] to investigate the progressive failure of a reinforced concrete frame subjected to the loss of an interior column. Corley et al. [14] and Yap and Li [6] indicated that seismic detailing may help to enhance the progressive collapse resistance mechanism. Unfortunately, the experimental work is expensive, time consuming, and non-repeatable. In that case, numerical and theoretical models have emerged as suitable substitutes for analyzing the structures under progressive collapse.

A computer analysis program presented by Gross and McGuire [15] is capable of tracing collapse nature of framed structures. This research is one of the first theoretical studies on progressive collapse. 2D RC frame was also used in Casciati and Faravelli [16] study to investigate the seismic reliability in progressive collapse scheme. A new modeling method is proposed by Weng et al. [17] for

progressive collapse analysis of 2D reinforced concrete frame under the loss of single or multiple columns. For this, the effect of service loads was incorporated before column removal into the analysis. Progressive collapse analysis is a complicated phenomenon. Most of the recent study proposed simpler models for simulation of progressive collapse. Moreover, Jian and Zheng [18] developed a simplified model to study the response of reinforced concrete beam column substructures under mid span point loading. Three dimensional non-linear numerical studies of precast concrete floor joints are carried out by Tohidi et al. [19] to simulate the ductility behavior in underlying wall supports removal scenario. In this study, the interfacial bond behavior between the steel and the grout were established by using translator elements embedded in ABAQUS. Sasani et al. [20] proposed a model that accounts for bar fracture of reinforced concrete frame structures. Furthermore, Naji [21] developed model using limit to investigate the effect of catenary action on resistance mechanism of progressive collapse. The main objectives of this study is to investigate the effects of the percentage of beam top and bottom reinforcement bars and beam span-to-depth ratio on resisting mechanism of progressive collapse. For this purpose different RC sub-assemblage finite element models are developed each having two beams, one middle column stub and two end column stubs and the mechanism of progressive collapse resistance under mid span point loading is analyzed in different stages of deflections. A computational study of the structural behavior under progressive collapse event described in this paper is accomplished using nonlinear static procedures in ABAQUS.

MECHANISM OF PROGRESSIVE COLLAPSE RESISTANCE

The characteristics features of different types of collapse as classified by Starossek [22] are the initial failure of one or a few load carrying elements, the redistribution of forces by alternate load path, static and dynamic force concentration in adjacent elements to fail next, and failure progression in vertical direction. Generally structures are designed with the seismic philosophy of strong column and weak beam. The beam column connection of reinforced concrete frames are designed with the negative bending moments before the middle column is removed. Following a sudden loss of middle column in progressive collapse event, the bending moments in the double span beams over the missing column are severely increased and the beam column connections just above the missing column have to carry the large positive bending moments as shown in Figure 1. If the affected beam-slab structures failed to sustain the increased bending moments, alternate load paths are required to eliminate the occurrence of progressive collapse.

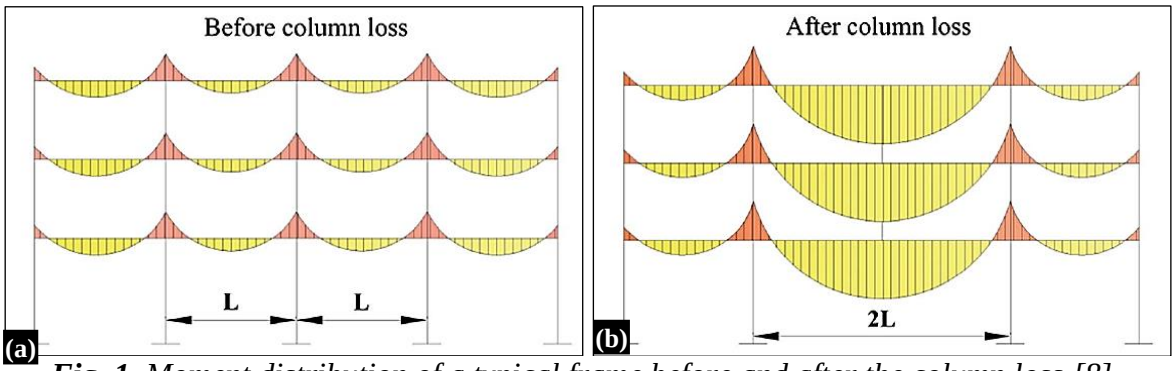

Fig. 1. *Moment distribution of a typical frame before and after the column loss [8].*

In a common progressive collapse event where a vertical element is lost, there exits three critical load resisting mechanisms - beam mechanism stage, transient stage and catenary mechanism stage as shown in Figure 2. Line OAB represents the beam mechanism stage. Initially all beams are able to sustain the vertical loads through flexural action (FA) which they are design for. Compressive arch action (CAA) provides additional flexural strength due to axial lateral restraint. Initially the only the beam action is considered to withstand the applied load in transient stage. Point C is the critical state at which the beam reaches ultimate moment, which is determined as a 15% reduction of the maximum moment (Li et al. [23]. Point D shows that the ultimate state of catenary action. During catenary mechanism stage, flexural action contributes almost zero resistance and the reinforcement bars through the whole span develops tensile resistance to resist applied load. Moreover, catenary action is the mechanism by which the structure redistributes the load carried by the failed member to the adjacent members through axial tension force induced in the bridging beams at large displacement Bao et al. [24]. In the recent years the research community has paid more attention towards the secondary mechanisms in double span beams bridging over the failed vertical structural element, namely, compressive arch action and catenary action.

FINITE ELEMENT MODELING

In order to investigate the structural behavior of sub-assemblages under column removal scenario, the analysis is carried out using ABAQUS 2017. Model of specimen M4 is developed considering the same geometric, material properties and boundary conditions as specimen S4 [7] used in the experimental program. Also six models are developed varying the geometric properties, bottom reinforcement ratio, top reinforcement ratio and span-to-depth ratio with the control model M4 as shown in Table 1. Top Reinforcement Ratio (TRR) and Bottom Reinforcement Ratio (BRR) at the middle joint interfaces play a crucial role after a middle column is removed in progressive collapse scenario. Therefore, FE models M6-2, M6-3 and M4, M5 and M5, M6-2 and M4, M6-3 are used to study the effects of BRR and TRR ratio at the middle joint interfaces respectively, on structural behavior.

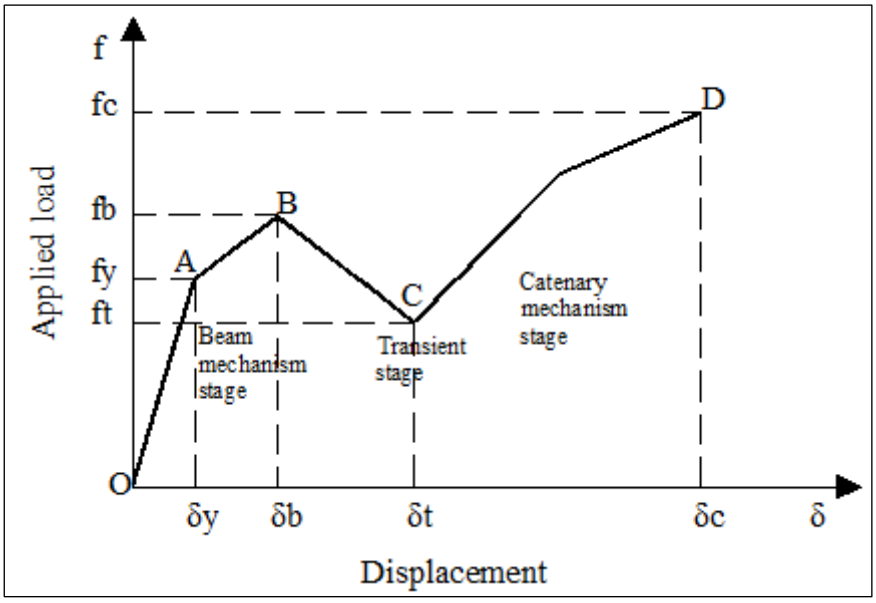

Fig. 2. *Applied load vs. displacement.*

Table 1. *Geometric properties of FE model beam-column Sub-assemblage.*

FE model	Beam span (mm)	Beam section (b mm x h mm)	L/h	Position of curtailment for beam top bar near joints (mm)	Longitudinal reinforcement			
					At beam end joints		*At beam span*	
					Top	Bottom	Top	Bottom
M4	2,750	150 x 250	23	1,000	3T13 (1.24%)	2T13 (0.82%)	2T13 (0.82%)	2T13 (0.82%)
M5	2,750	150 x 250	23	1,000	3T13 (1.24%)	3T13 (1.24%)	2T13 (0.82%)	3T13 (1.24%)
M6-2	2,750	150 x 250	23	1,000	3T16 (1.87%)	3T13 (1.24%)	2T16 (1.25%)	3T13 (1.24%)
M6-3	2,750	150 x 250	23	1,000	3T16 (1.87%)	2T13 (0.82%)	2T16 (1.25%)	2T13 (0.82%)
M7	2,150	150 x 250	18.2	780	3T13 (1.24%)	2T13 (0.82%)	2T13 (0.82%)	2T13 (0.82%)
M8	1,550	150 x 250	13.4	560	3T13 (1.24%)	2T13 (0.82%)	2T13 (0.82%)	2T13 (0.82%)

Table 2. *Material properties of steel reinforcement.*

Bar type	Yield strength f_y (MPa)	Elastic modulus E_0 (MPa)	Strain at the start of hardening ε_{sh} (%)	Tensile strength f_u (MPa)	Ultimate strength ε_u (%)
R6	349	199,177	-	459	-
T10	511	211,020	2.51	622	11.00
T13	494	185,873	2.66	593	10.92
T16	513	184,423	2.87	612	13.43

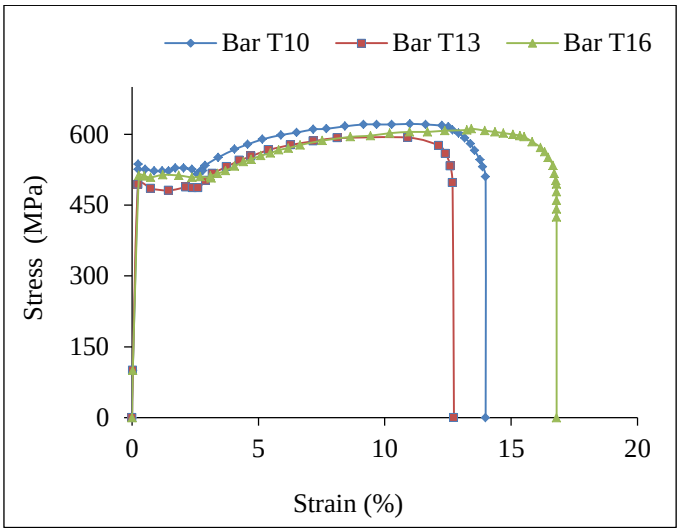

Fig. 3. *Stress-strain curve.*

Test conducted by Su et al. [25] under a middle column removal scenario concluded that the beam span-to-depth ratio is a key parameter which affects the structural behavior, particularly for CAA. Hence FE models M7 and M8 are developed with only vary in net span length than that of FE model M4 to investigate the effect of the beam span-to-depth ratio on structural behavior.

Material Models for Reinforcement

Compared with concrete, material properties of steel can be easily obtained from standard tensile test, since steel is a homogeneous material and have similar behavior in compression and tension. In this study the reinforcement bars are embedded in concrete material. The stress strain curves shown in Figure 3 are used to define steel properties. More details of the reinforcement bars used in this model are available in Table 2. Generally the Poisson's ratio of structural steel is accepted as 0.3.

Material Models for Concrete

ABAQUS facilitates for simulating the concrete damage using concrete damage plasticity model (CDPM). CDPM assumes

tensile cracking and compressive crushing as failure mechanism in concrete. Hence CDPM will be useful to develop a proper damage simulation model for analyzing any RC structures under both static and dynamic loading [26]. In this study this technique is applied to represent complete inelastic behavior of concrete both in compression and tension along with damage characteristics. The detail of material properties of concrete is available in Table 3. The complete stress-strain compressive curve of concrete is derived using Popovics [27] model and tensile curve is developed using Belarbi et al. [28].

Table 3. *Properties of concrete.*

Material	Initial modulus of elasticity, GPa	Compressive strength, MPa	Tensile strength, MPa
Concrete	29.6	38.2	3.5

Tensile Behavior

Figure 4(a) is used in ABAQUS to represent a post failure stress-strain relationship for concrete subjected to tension. The tensile stress-strain relationship generated by following Equation (1) from Chinese design code of reinforced concrete structure [29] and implemented in CDP model.

$$\sigma_t = \begin{cases} \rho_t(1.2 - 0.2x^5)E_c\varepsilon \; x \leq 1 \\ \frac{\rho_t}{\alpha_t(x-1)^{1.7}+x}E_c\varepsilon \; x > 1 \end{cases} \quad (1)$$

Where σ_t and ε represents the tensile stress and strain respectively,$x = \frac{\varepsilon}{\varepsilon_t}$,$\rho_t = \frac{f_t}{E_c\varepsilon_t}$, and f_t and ε_t represents peak tensile strength and strain and α_t represents the coefficient for the descending part.

In order to develop this model, young's modulus (E_0), yield stress (σ_t), cracking strain ($\tilde{\varepsilon}_t^{ck}$) and damage parameter ($d_t$) values should be input by user for the relevant grade of concrete. The cracking strain is calculated as,

$$\tilde{\varepsilon}_t^{ck} = \varepsilon_t - \varepsilon_{ot}^{el} \quad (2)$$

Where,$\varepsilon_{ot}^{el} = \frac{\sigma_t}{E_0}$ Elastic strain corresponding to undamaged material, ε_t = total tensile strain. Figure 4(b) represents a tensile damage curve used in this model. The plastic strain value as calculated in Equation (3) is used to check accuracy of damage curve in ABAQUS, which indicates an error if the values of plastic strain are decreasing [26].

$$\tilde{\varepsilon}_t^{pl} = \tilde{\varepsilon}_t^{ck} - \frac{d_t}{(1-d_t)}\frac{\sigma_t}{E_0} \quad (3)$$

Compressive Behavior

Figure 5(a) represents the stress-strain relationship of concrete in compression. The compressive stress-strain relationship is generated following Equation (4) from Chinese design code of reinforced concrete structure [29] and implemented in CDP model.

$$\sigma_c = \begin{cases} \frac{\rho_c n}{n-1+x^n}E_c\varepsilon \; x \leq 1 \\ \frac{\rho_c}{\alpha_c(x-1)^2+x}E_c\varepsilon \; x > 1 \end{cases} \quad (4)$$

Where σ_c and ε represents the compressive stress and strain respectively,$x = \frac{\varepsilon}{\varepsilon_c}$, $\rho_c = \frac{f_c}{E_c\varepsilon_c}$, $n = \frac{E_c\varepsilon_c}{E_c\varepsilon_c - f_c}$, f_c, ε_c and E_c represents peak compressive stress and strain and elastic modulus of concrete and α_c represents the coefficient for the descending part.

To develop this relationship user needs to input the value of yield stresses (σ_c) along with inelastic strains ($\tilde{\varepsilon}_c^{in}$), calculated as in Equation (5) corresponds to yield stress. Figure 5(b) is the concrete compression damage curve, developed inputting damage parameter (d_c) and inelastic strain in tubular form.

$$\tilde{\varepsilon}_c^{in} = \varepsilon_c - \varepsilon_{oc}^{el} \quad (5)$$

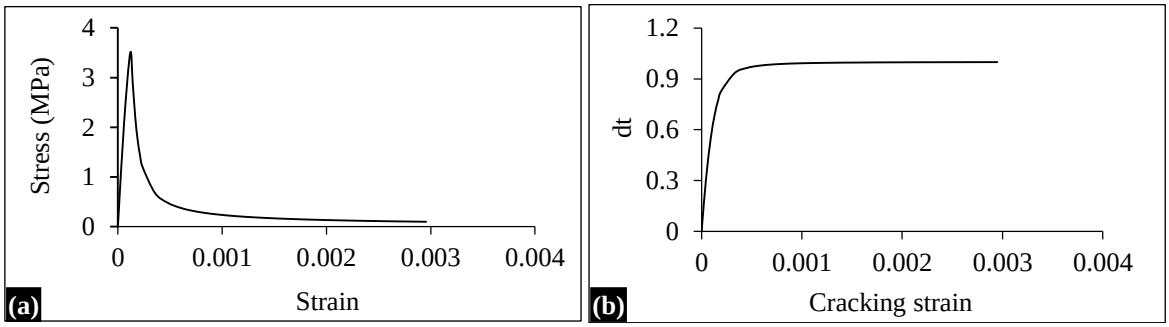

Fig. 4. *(a) Tensile Stress-strain relationship (b) Damage vs. inelastic strain.*

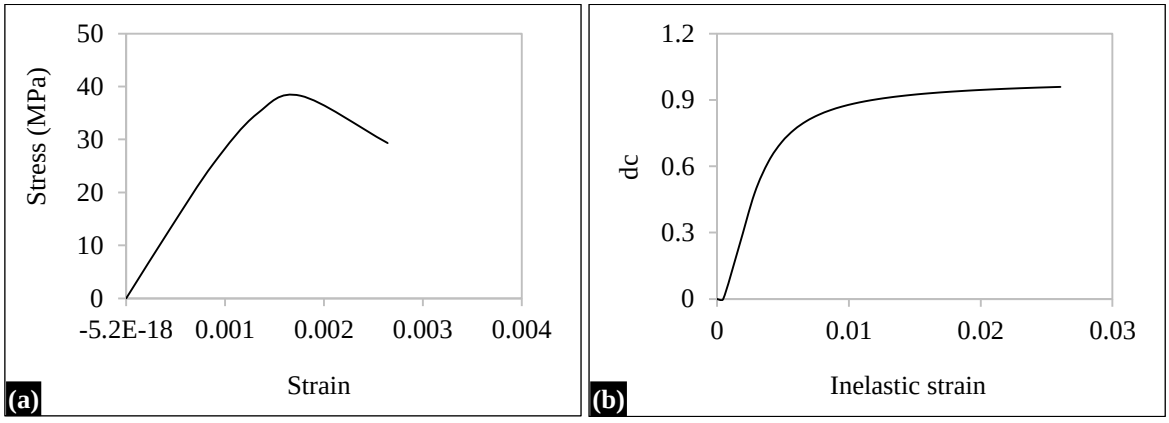

Fig. 5. *(a) Compressive Stress-strain relationship,(b) Damage vs. inelastic strain.*

Table 3. *Plasticity parameters for CDP model.*

Dilation Angle	Eccentricity	Fb0/fc0	K	Viscosity Parameter
20	0.1	1.16	0.6667	0.001

Where, $\varepsilon_{oc}^{el} = \frac{\sigma_c}{E_0}$Elastic strain corresponding to undamaged material, ε_c = total compressive strain. ABAQUS check the accuracy taking in account the plastic strain values ($\varepsilon_c^{\sim pl}$) calculated using Equation (6), which are neither negative nor decreasing with increased stresses [26].

$$\varepsilon_c^{\sim pl} = \varepsilon_c^{\sim in} - \frac{d_c}{(1-d_c)}\frac{\sigma_c}{E_0} \quad (6)$$

CDPM requires special parameters such as dilation angle, eccentricity, biaxial loading ratio, the coefficient K and viscosity parameter and these values are tabulated in Table 4. The convergence rate in the softening regime of concrete stress-strain curve can enhance by a lower viscosity parameter [30].

The embedded element model for concrete to steel interaction is useful for both static and dynamic analysis, and is applicable in linear and non-linear analysis of progressive collapse. Furthermore it is a full interaction without slippage [26]. Therefore, this technique is applied for this study as illustrated in Figure 6. Static loading is applied on the center of mid column stub via control displacement process. Moreover, boundary condition adopted for FE models is taken identical as in its experimental condition. 3D cubic element with eight nodes (C3D8R) and 3D truss element with two nodes (T3D2) are used for finite element modeling of concrete and steel bars respectively. Studies on mesh sensitivity in static analysis suggest that mesh size between 20 and 76 mm yields accurate outcomes for concrete pressure and tension [24].

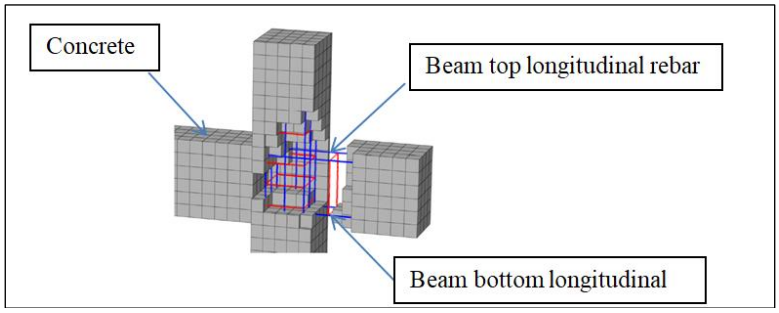

Fig. 6. *Embedded rebar inside concrete.*

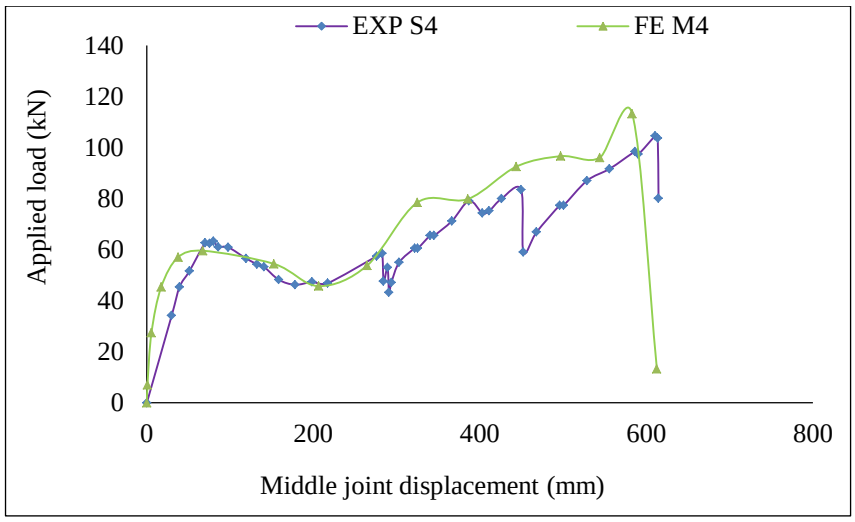

Fig. 7. *Finite element models in comparison to experimental specimen.*

For this study the FE model mesh are selected as 50mm via several trials with different mesh size and comparing the outcomes with experimental results.

MODEL VALIDATION

Figure 7 represents the curves of applied vertical load verses the vertical displacement of middle column obtained from test and the finite element model. The curves shows that the vertical displacement of the middle column obtained from the FE model is in good agreement with the test results in all three phases of progressive collapse resistance i.e., flexural, CAA and catenary action, and the course of development of the applied load obtained from the FE model and text is similar. Figure 8 (a) and (b) represents the local failure modes shown by FE model and experiment at the beam ends respectively. The sudden drop for the resisting force as observed in the Figure 7 is due to the fracture of beam bottom reinforcement bars near the middle column stub as shown in Figure 9. The occurrence of fracture of beam top reinforcement bars on FE model M4 is found similar with test results. However, there occurs the deviation in time of first and second bottom bar fracture. This deviation may be due to the loading speed, mesh size and the type of analysis adopted. In addition, a full interaction between concrete and reinforcement bars without slippage may vary the time of rebar fracture in FE model from experimental results.

APPLIED LOAD VERSUS MIDDLE JOINT DISPLACEMENT

Figure 2 and Figure 7 represent the generalized curve of force verses displacement in progressive collapse events.

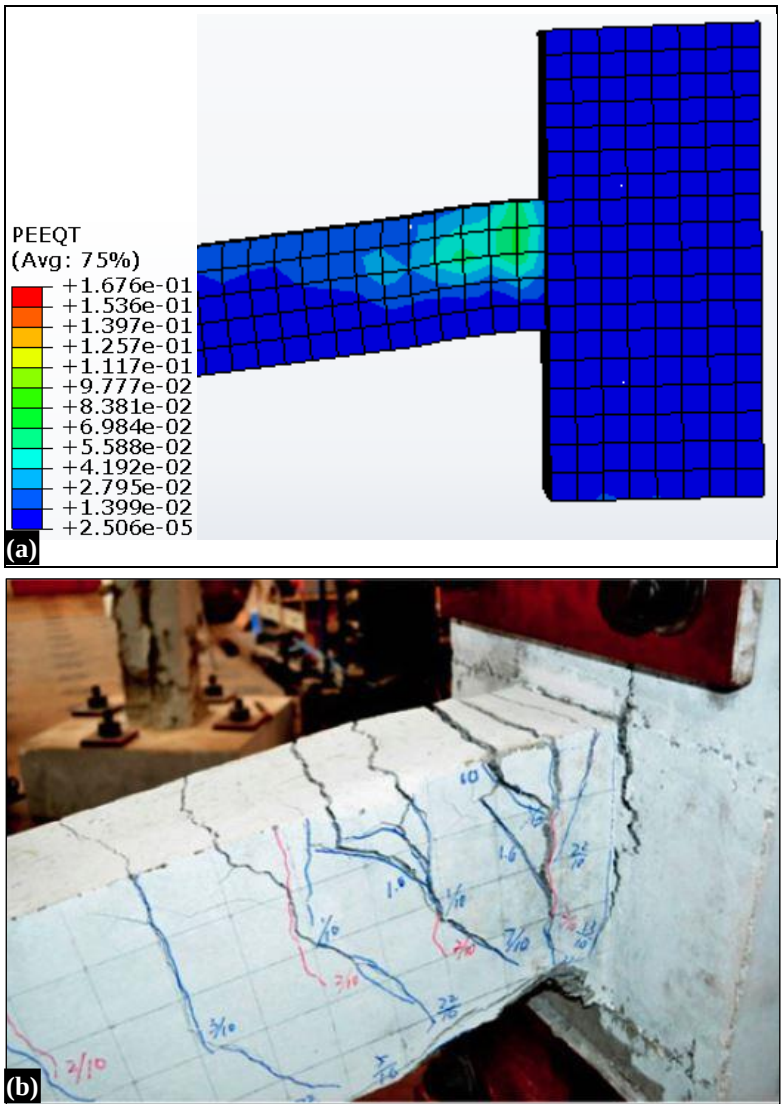

Fig. 8. *Local failure modes at the beam end (a) FE model M4, (b) experiment.*

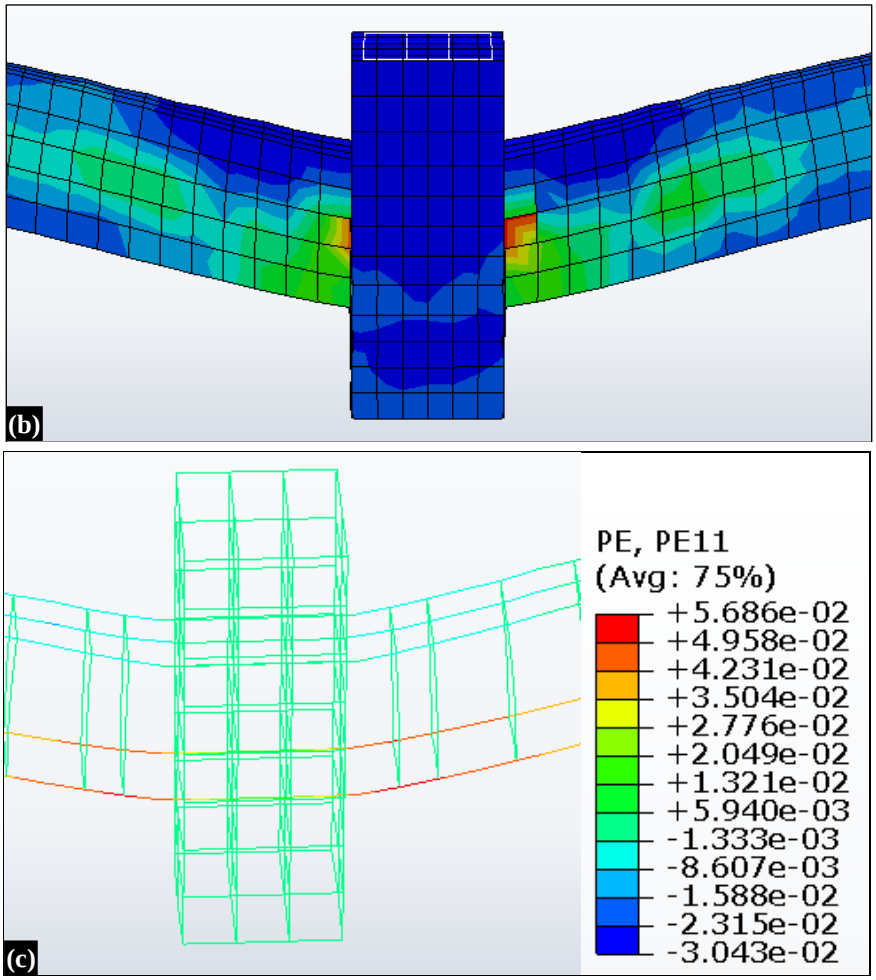

Fig. 9. *Local failure modes at the middle joint regions (a) experiment, (b) FE model M4 and (c) PE11 of FE model M4 showing fracture of rebar at the end of CA.*

Initially all beams mobilize the flexural action to sustain the vertical loads in the primary stage of column removal event. Prior to the loss of middle column, the bottom rebar in the vicinity of middle joint is in elastic compression at service loads. The bottom rebar is unloaded in compression after the middle column has been removed and again reloaded in tension up to yielding. The ascending portion of the curve represents the elastic stage. The inelastic stage begins once the cracking of beam is observed and the curve descends after reaching the peak load until the bottom bar ruptures. At the end of this stage most of the steel bars has yielded at beam ends near the missing column, indicating the formation of plastic hinges in the beams. The beams then begin to act like cables on larger deflections which further activate catenary action. Furthermore, catenary action provided by the top reinforcement is only the primary resisting mechanism at large deflections, characterized by the ascending portion of curve at the later stage. The overall performance of the sub-assemblage is described by the applied load verses middle joint deflection curve. In addition, the beams deflected symmetrically at both sides of the lost column in case of FE model M4 which can be illustrated by the displacement at specific points along the beam span different stages of loading as shown in Figure 10. Also it can be noticed that there is a wide gap in displacement between the first and second fracture of beam bottom reinforcement bar. This large

difference in displacement may be due to the formation of plastic hinge at the middle joint.

FAILURE MODES OF FE MODELS

The similar failure modes are obtained for all the FE models, for simplicity, FE model M4 is singled out to examine the failure modes. However, those of FE model M8 shows different structural mechanism than other FE models. The load-displacement history of each FE models reflects that the crushing of concrete and the bottom and top reinforcement bar fracture, are primarily concentrated at the beam-column joints. At a small displacement, the flexural cracks are observed at the bottom of beam near middle joints and at the top of beam end joints for all FE models. Beyond the flexural capacity, further increase in resisting load is observed due to activation of CAA and the load continue increasing till the end of CAA which is also explained by the Figure 11(a). On further increase in displacement corresponding to yield stress, the resistance force decreases steadily showing the ends of flexural and CAA capacity, as explained in Figure 11(b) and (c). Other than FE model M8, when the displacement exceeded the depth of the beam, beam mechanism is replaced by catenary mechanism which further increased the loadtill the beam top reinforcement bar gets fractured followed by the fracture of beam bottom reinforcement bars. The force verses deflection curve obtained from M8 model in Figure 14 demonstrates that structures are likely to mitigate the progressive collapse via CAA even though catenary action is mobilized.

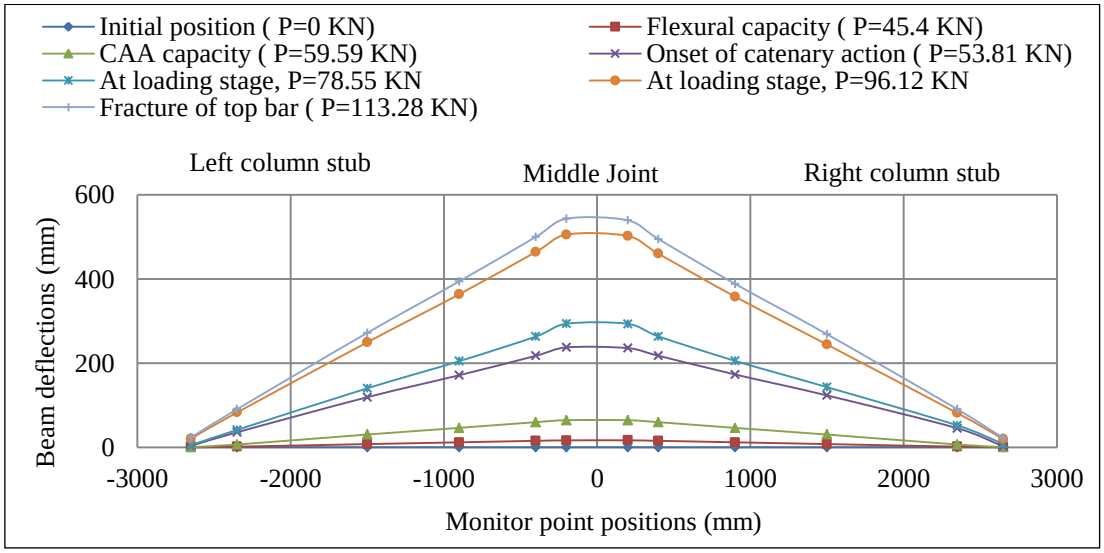

Fig. 10. *Overall deflection curves of Specimen M4.*

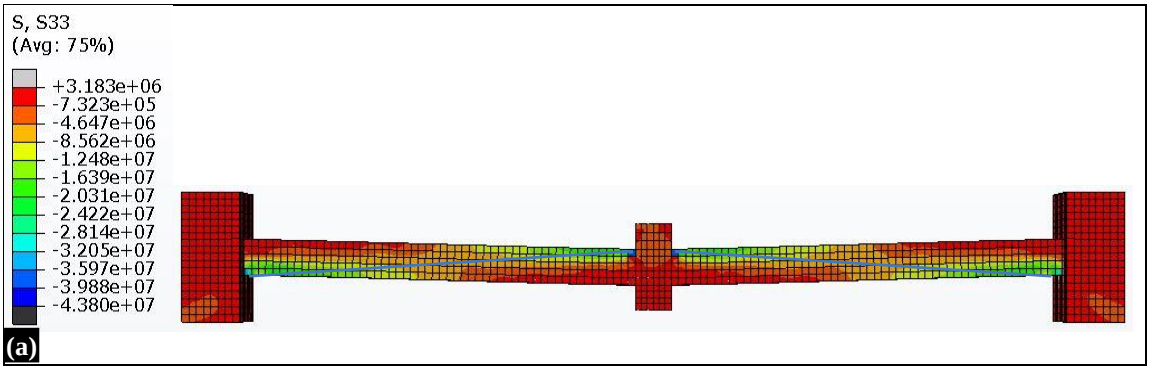

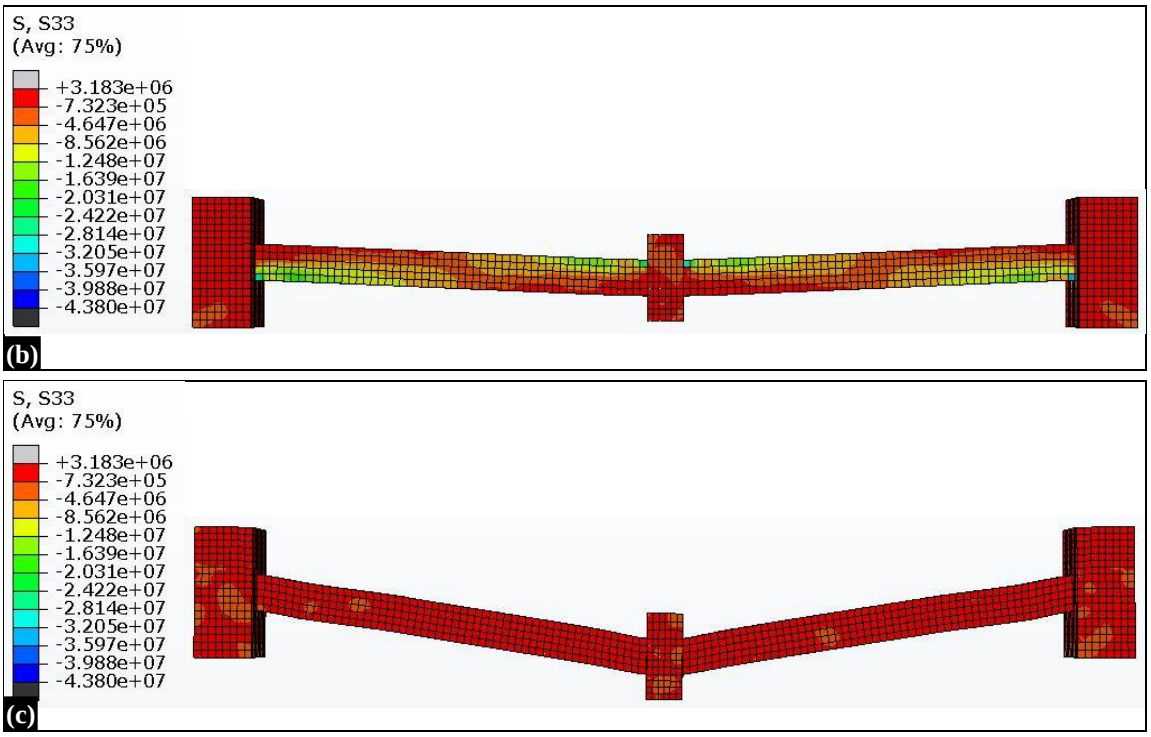

Fig. 11. *FE model M4 (a) Start of CAA; (b) Reduction of CAA with load increase; (c) End of CAA.*

Effect of the Bottom Reinforcement Ratio at Middle Joints on Structural Behavior

Applied load verse middle joint displacement plots of FE models M4 and M5 and M6-2 and M6-3 in Figure 12 are compared to investigate the effects of BRR at the ends of beams adjacent to the missing column on overall structural behavior of sub-assemblages. With the same TRR i.e., 1.24% for M4 and M5, the results shows that for the same deflection, increase in BRR will provide higher structural resistance in the compressive arch action and initial stage of catenary action. Hence higher structural resistance against progressive collapse can be achieved with increase in BRR at a relatively smaller displacement. For FE model M5, the catenary action attained a resistance of 104.66 KN before the fracture of first bottom bar occurred, around 48.3% greater than the CAA capacity of 70.6 KN as shown in Table 5. However the CAA and the catenary action resistance prior to the beam first bottom bar fracture of FE model M4 is lower than the FE model M5. Similarly FE model M6-2 with BRR 1.24% shows higher structural resistance in CAA than FE model M6-3 with BRR 0.82%. The load for the beam first bottom bar fracture is almost same but FE model M6-2 attains higher deflection. Similarly the peak load at catenary action in FE model M6-2 is higher than the FE model M6-3.

Effect of the Top Reinforcement Ratio at Middle Joints on Structural Behavior

Figure 13 compares the effects of top reinforcement ratio at the joints on the overall structural behavior of RC FE models M5 and M6-2 and M4 and M6-3 respectively. The bottom reinforcement ratios for FE model M5 and M6-2 is same i.e., 1.24% and for FE model M4 and M6-3 is same i.e., 0.82%. A comparison of FE models M5 and M6-2 and M4 and M6-3 in Table 5 shows that with an increase in TRR, a higher resistance is obtained in CAA.

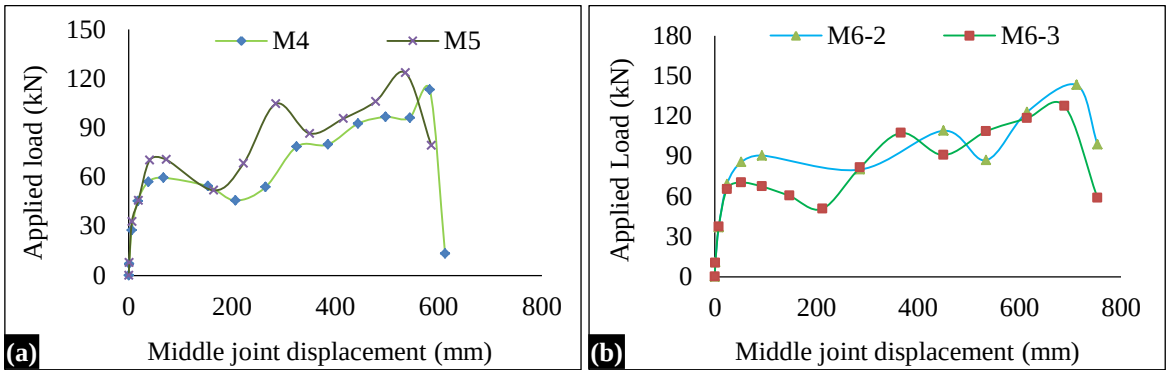

Fig. 12. *Effect of BRR at the middle joint on the structural behavior of RC beam column sub-assemblages.*

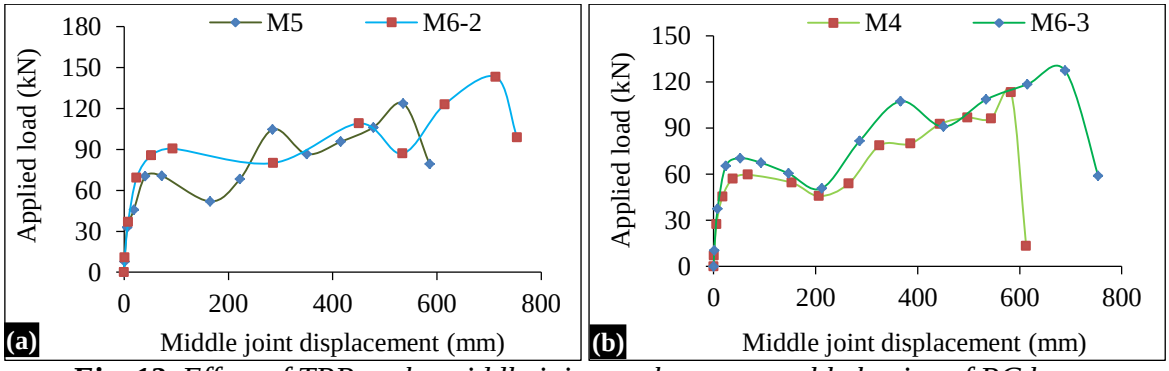

Fig. 13. *Effect of TRR at the middle joint on the structural behavior of RC beam column sub-assemblages.*

Table 4. *Finite element modeling results at critical stages.*

Specimens	Peak Load at CAA		Beginning of CA		Catenary Stage	
	Max. Load, KN	*MJD mm*	*Load KN*	*MJD mm*	*Max. Load KN*	*MJD mm*
M4	59.6	67.32	45.73	206.42	113.28	582.88
M5	70.6	72.49	51.88	164.68	123.57	535.55
M6-3	70.36	52.13	50.72	211.78	127.36	688.8
M6-2	90.523	93.17	80.03	285.88	143.16	712.65
M7	89.95	51.85	60.97	117.52	104.53	697.54
M8	147.708	13.3	72.63	117.71	119.27	470.75

The peak load at CAA for FE model M6-2 is 90.52 KN which is 28.2% higher than FE model M5 i.e., 70.6 KN. Likewise, peak load at CAA for FE model M6-3 is 70.36 KN which is 18% higher than FE model M4 i.e., 59.59 KN. Also resistance at the first fracture of the bottom bars is found higher with an increase in TRR. The capacity of catenary action for FE models M6-2 is higher than M5 with larger displacement.

Effect of the Beam Span-To-Depth Ratio on Structural Behavior

Figure 14 show that the beam span-to-depth ratio fundamentally affects the performance of structure on progressive collapse event. It is because FE model M8 with lowest span-to-depth ratio could only provide resistance at CAA stage and failed to provide structural resistance through catenary action. Although FE model M7 (4.55m) is shorter in length than FE model M4 (5.75m), it follows the similar failure mode as Fe model M4. When further reduction in beam span length, it shows that FE model M8 (3.35m) follows different structural mechanism. Furthermore, it suggests that there is a brink beam span-to-depth ratio that affects

the structural mechanism, such as catenary action. Hence it demonstrates that with short beam span-to-depth ratio, a higher resistance is provided to the structure through CAA rather than catenary action.

STRAIN VARIATION

Figure 15 shows the strain variation in rebar in beam of FE model M4. It is observed that the rebar in the top of left and right end of the beam are in tension, whereas, the rebar in the bottom of left and right end of the beam are in compression which is also illustrated by Figure 16(a) and (b). It is also observed that the strain in rebar in the top of left and right end is same up to the compressive stage but strain in rebar in top of right end gradually increases in tension than strain in rebar in top of left end after the compressive stage. However, the strain in rebar in the bottom of right and left end varies from early stage of loading. Furthermore, the strain in rebar in the top of the middle joint is in compression and the strain in rebar in the bottom of the middle joint is in tension as illustrated in Figure 16(a) and (b). The strain in concrete with increase in load is shown in Figure 17.

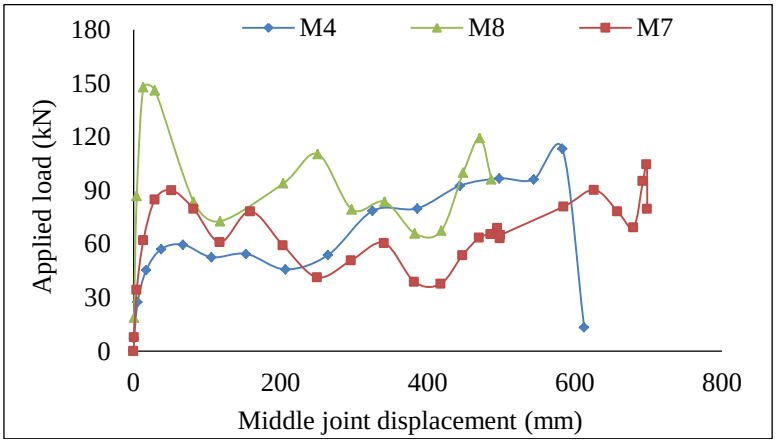

Fig. 14. *Effect of beam span-to-depth ratio at the middle joint on the structural behavior of RC beam column sub-assemblages.*

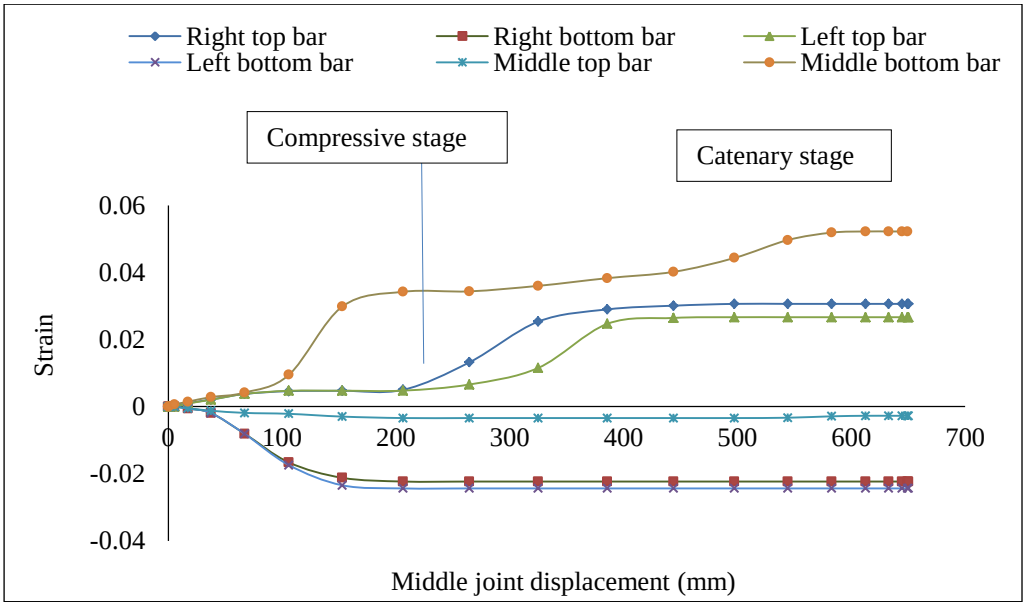

Fig. 15. *Strain in rebar in beam of FE model M4.*

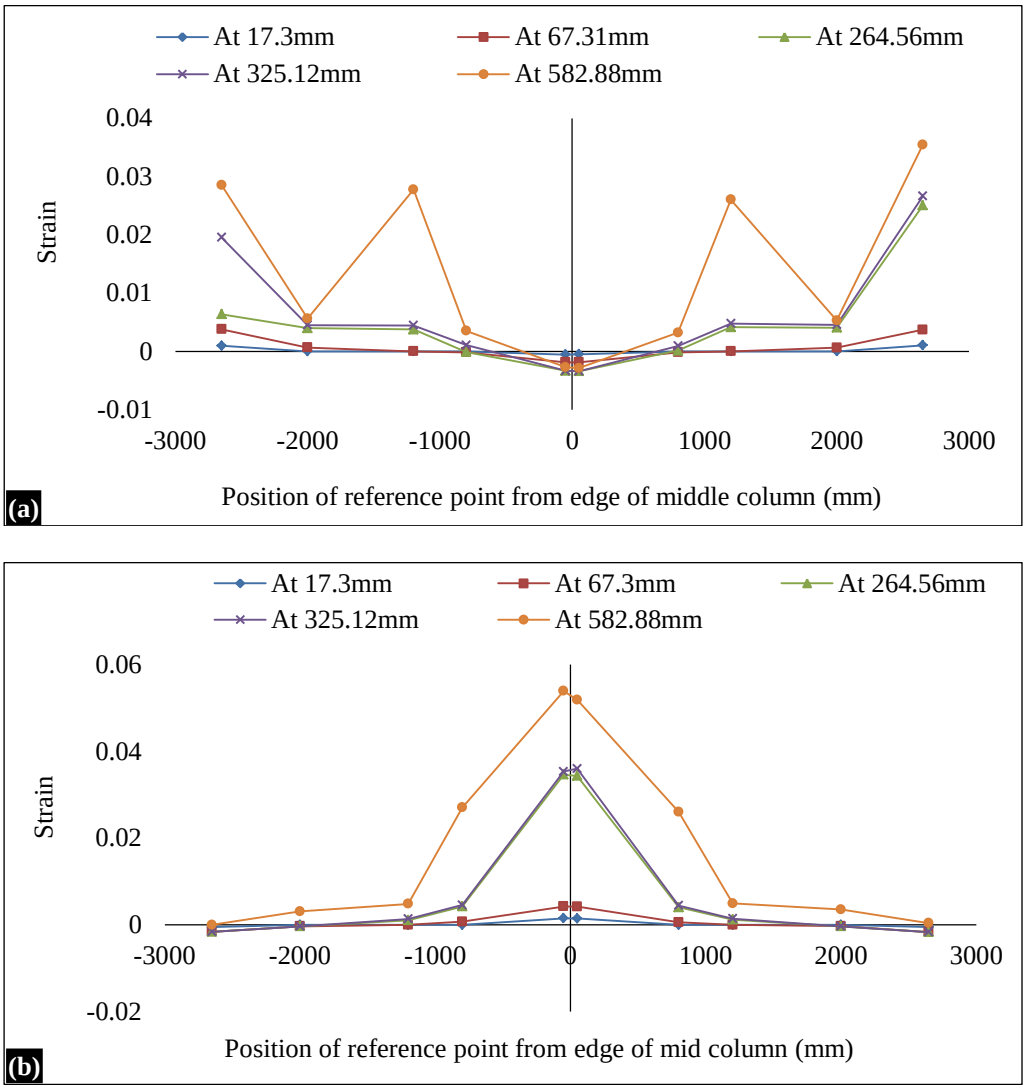

Fig. 16. *Variations of longitudinal reinforcement strain of M4 (a) Strain in top longitudinal beam rebar, (b) Strain in bottom longitudinal beam rebar.*

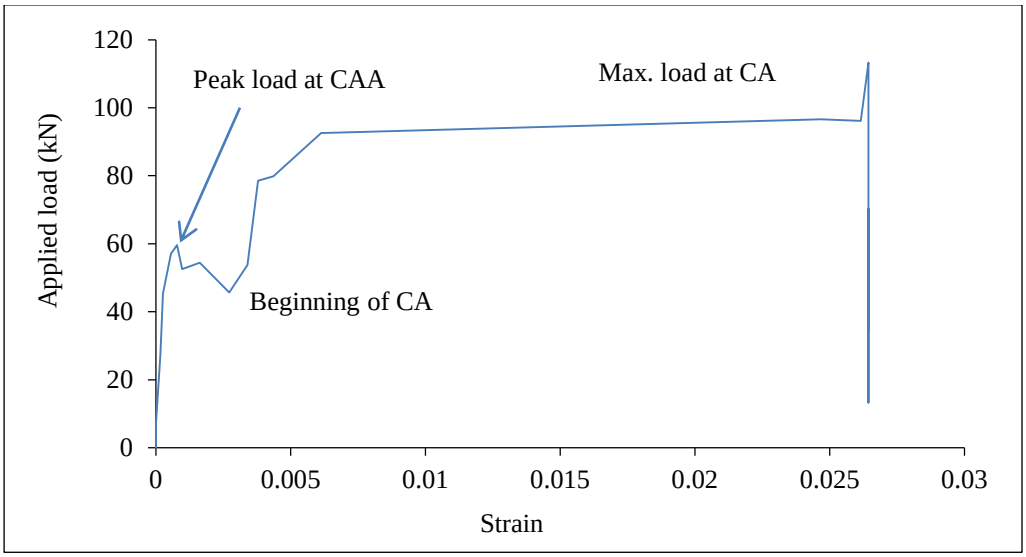

Fig. 17. *Vertical Applied load verses concrete strain at middle joint interface.*

AXIAL STRESS VERSES MIDDLE JOINT DISPLACEMENT

The plot of axial stress verses middle joint displacement in Figure 18 and Figure 19(a) and (b) illustrates that the top longitudinal reinforcement at left and right end and the bottom longitudinal reinforcement at the middle joint are always in tension. However, it also illustrate that the bottom longitudinal reinforcement at left and right end and the top longitudinal reinforcement at the middle joint are in compression throughout the beam mechanism and compressive arch action stage and gradually changes from compression to tension in the catenary action stage. Moreover, the top longitudinal reinforcement at the middle joint change from compression to tension when the vertical displacement reached around 265mm, whereas, the bottom longitudinal reinforcement at left and right end changes when the vertical displacement reached about 335mm.

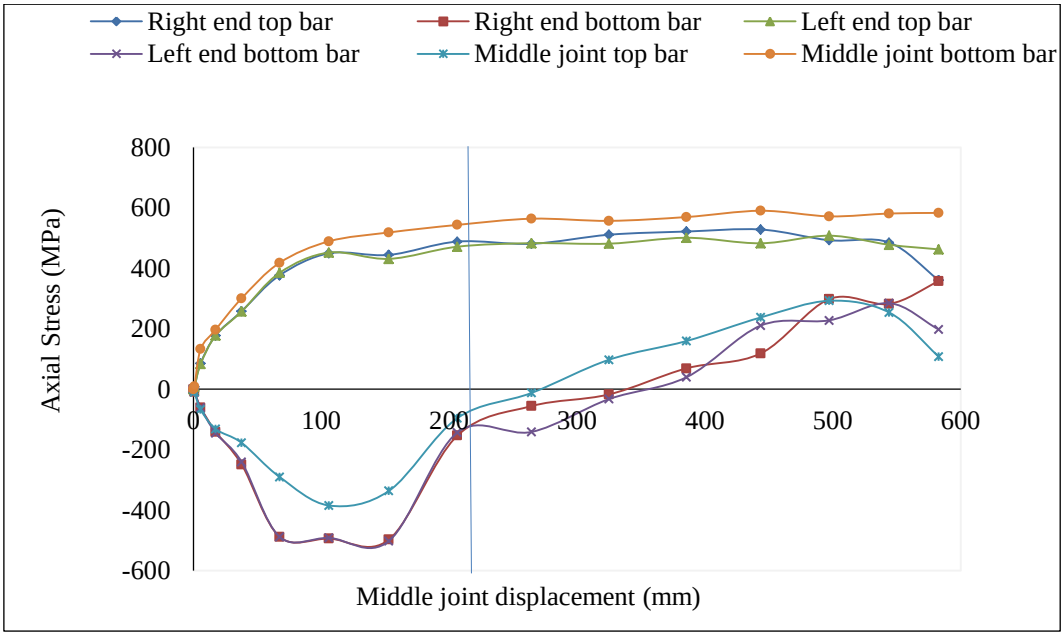

Fig. 17. *Axial stress of beam longitudinal top and bottom reinforcement of M4.*

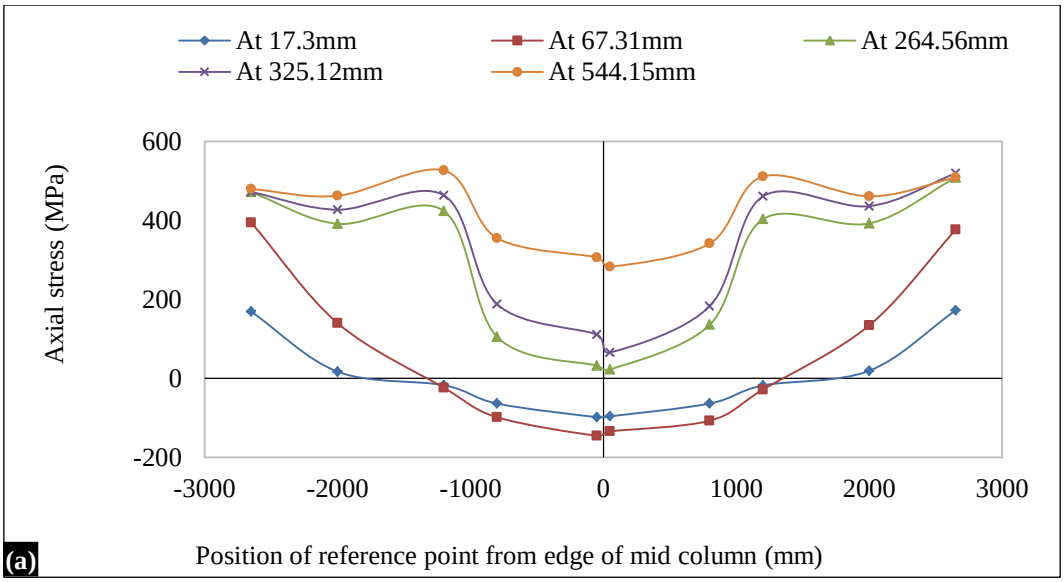

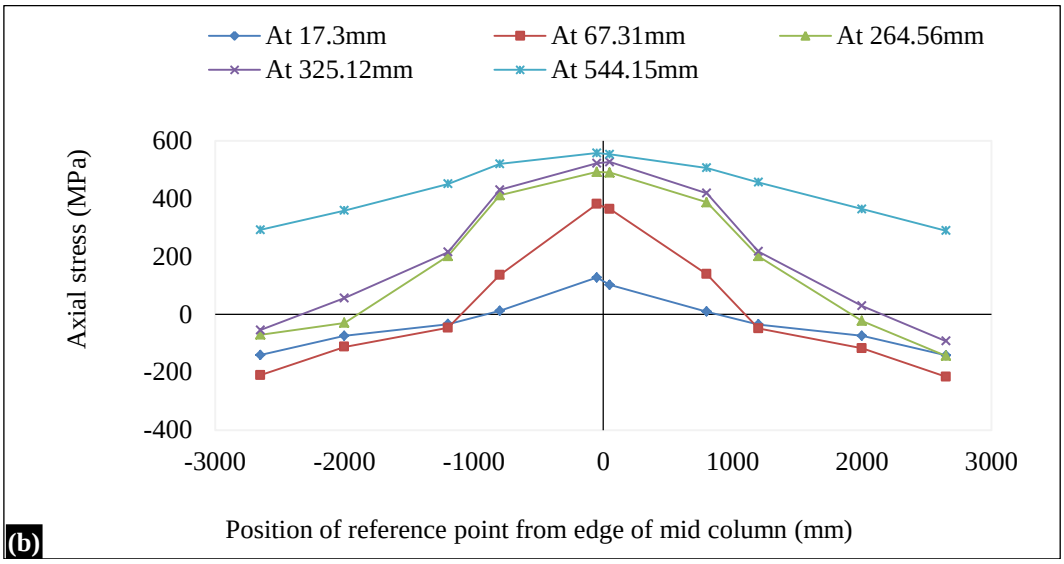

Fig. 18. *Variations of longitudinal reinforcement stress of M4 Stress in top longitudinal beam rebar, (b) Stress in bottom longitudinal beam rebar.*

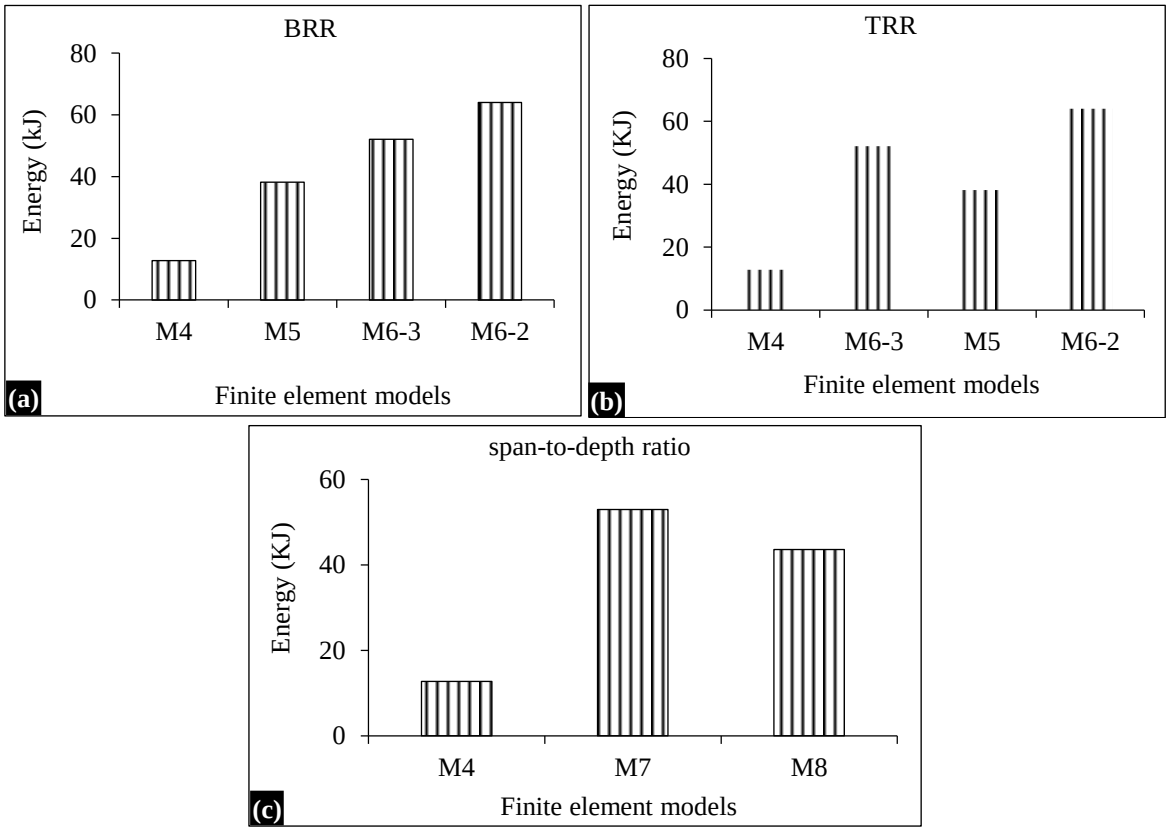

Fig. 19. *Energy absorption capacity of FE models.*

ENERGY ABSORPTION

Higher in energy absorption capacity can provide higher resistance to progressive collapse of structure. In other words, RC structures require significant energy absorption capacity to avoid progressive collapse and restrict the local damage from spread throughout the structure. Energy absorption capacity of FE models with BRR 1.24% (M5 and M6-2) is higher than

FE models BRR 0.82% (M4 and M6-3). Likewise, the energy absorption capacity of FE models with TRR 1.87% (M6-2 and M6-3) is higher than FE models with TRR 1.24% (M4 and M5) as observed in Figure 20. This is due to increase structural resistance mainly in the CAA stage. Hence, it shows that increase in BRR and TRR, the energy absorption capacity is increased which helps to prevent from spreading the local damage throughout the structure in progressive collapse event. It also reveals that shorter beam span-to-depth ratio enhances the energy absorption capacity as compared to FE model M4 with L/h ratio 23 and FE model M7 with L/h ratio 18.2. However, on further decrease in L/h ratio as in FE model M8 i.e., 13.4, energy absorption capacity is decreased as compared with FE model M7 indicating that there exists the threshold beam L/h ratio that determines the structural mechanism.

CONCLUSION

- A simplified model is developed to investigate the structural behavior of RC beam column sub-assemblages under a middle column removal scenario and its reliability is verified by experimental results in literature. Therefore, the proposed model is able to predict the capacity of structural resistance to collapse at beam mechanism stage and catenary action stage with satisfactory accuracy.
- With increase in BRR, higher resistance against progressive collapse can be obtained at a relatively smaller displacement whereas higher TRR can significantly increase the structural resistance of beam column sub-assemblages in CAA and first fracture of bottom reinforcement.
- Beam column sub-assemblages with lower L/h ratio significantly increase the structural resistance contributed by CAA whereas catenary action can significantly enhance the progressive collapse resistant mechanism with higher L/h ratio.
- There exists the threshold beam span-to-depth ratio that affects the structural mechanism, such as catenary action.
- Considering high expense of experimental works, time consuming, experimental errors and non-repeatable work, the finite element model proposed in this study can provide an optimal solution for estimating the structural behavior of RC beam column sub-assemblages subjected to a progressive collapse. However, progressive collapse is a complex phenomenon; the proposed simplified finite element model should be validated by more experiments or numerical analysis.

REFERENCES

[1] GSA. Progressive Collapse Analysis and Design Guidelines for New Federal Office Buildings and Major Modernization Projects. US General Services Administration 2003.

[2] ICC. International Building Code. Falls Church (VA). International Code Council 2009.

[3] ACI Committee 318. Building Code Requirements for Structural Concrete and Commentry 2011.

[4] DoD. Design of buildings to resist progressive collapse. Unified Facilities Criteria (UFC) 4-023-03 2009.

[5] Qian K, Li B. Experimental and Analytical Assessment on RC Interior Beam-Column Subassemblages for Progressive Collapse. Journal of Performance of Constructed Facilities 2012;26:576–89. doi:10.1061/(ASCE) CF.1943-5509.0000284.

[6] Yap SL, Li B. Experimental investigation of reinforced concrete exterior beam-column subassemblages for progressive collapse. ACI Structural Journal 2011;108:542–52. doi:10.14359/51683211.

[7] Yu J, Tan KH. Structural Behavior of RC Beam-Column Subassemblages under a Middle Column Removal Scenario. Journal of Structural Engineering 2013;139:233–50. doi: 10.1061/(ASCE)ST.1943-541X.0000658.

[8] Alogla K, Weekes L, Augusthus-nelson L. A new mitigation scheme to resist progressive collapse of RC structures. Construction and Building Materials 2016;125:533–45. doi:10. 1016/j.conbuildmat.2016.08.084.

[9] Rashidian O, Abbasnia R, Ahmadi R, Mohajeri Nav F. Progressive Collapse of Exterior Reinforced Concrete Beam–Column Sub-assemblages: Considering the Effects of a Transverse Frame. International Journal of Concrete Structures and Materials 2016;10:479–97. doi:10. 1007/s40069-016-0167-2.

[10] Yu J, Tan KH. Special Detailing Techniques to Improve Structural Resistance against Progressive Collapse. Journal of Structural Engineering 2014;140:4013077. doi:10.1061/(ASCE)ST.1943-541X. 0000886.

[11] Lim NS, Tan KH, Lee CK. Experimental studies of 3D RC substructures under exterior and corner column removal scenarios. Engineering Structures 2017;150:409–27. doi:10.10 16/j.engstruct.2017.07.041.

[12] Sasani M, Bazan M, Sagiroglu S. Experimental and Analytical Progressive Collapse Evaluation of Actual Reinforced Concrete Structure 2008:731–40.

[13] Yi W-J, He Q-F, Xiao Y, Kunnath SK. Experimental Study on Progressive Collapse-Resistant Behavior of Reinforced Concrete Frame Structures. ACI Structural Journal 2008;105:433–9. doi:10.14359/19857.

[14] Corley WG, Sr. PFM, Sozen M a., Thornton CH. The Oklahoma City Bombing: Summary and Recommendations for Multihazard Mitigation. Journal of Performance of Constructed Facilities 1998;12:100–12. doi:10.1061/(ASCE)0887-3828 (1998)12:3(100).

[15] Gross JL, McGuire W. Progressive Collapse Resistant Design. Journal of Structural Engineering 1983;109:1–15. doi:10.1061/(ASCE)0733-9445 (1983)109:1(1).

[16] Casciati F, Faravelli L. Progressive failure for seismic reliability analysis. Engineering Structures 1984;6: 97–103.

[17] Weng J, Tan KH, Lee CK. Modeling progressive collapse of 2D reinforced concrete frames subject to column removal scenario. Engineering Structures 2017;141:126–43. doi:10.1016/j.engstruct.2017.03.018.

[18] Jian H, Zheng Y. Simplified Models of Progressive Collapse Response and Progressive Collapse-Resisting Capacity Curve of RC Beam-Column Substructures. Journal of Perfomance of Constructed Facilities 2014;28:1–7. doi:10.1061/(ASCE)CF.1943-5509.0000492.

[19] Tohidi M, Yang J, Baniotopoulos C. Numerical evaluations of codified design methods for progressive collapse resistance of precast concrete cross wall structures. Engineering Structures 2014;76:177–86. doi:10.1016/j.engstruct.2014.06.0 34.

[20] Sasani M, Werner A, Kazemi A. Bar fracture modeling in progressive collapse analysis of reinforced concrete structures. Engineering Structures 2011;33:401–9. doi:10.10 16/j.engstruct.2010.10.023.

[21] Naji A. Modelling the catenary effect in the progressive collapse analysis of concrete structures. Structural Concrete 2016;17. doi:10.1002/suco. 201500065.

[22] Starossek U. Typology of progressive collapse. Engineering Structures 2007;29:2302–7.
[23] Li Y, Lu X, Guan H, Ye L. An improved tie force method for progressive collapse resistance design of reinforced concrete frame structures Author Griffith Research Online Improved Tie Force Method for Progressive Collapse Resistance Design of RC. Engineering Structures 2011;33(10):2931–42.
[24] Bao Y, Lew HS, Kunnath SK. Modeling of Reinforced Concrete Assemblies under Column-Removal Scenario. Journal of Structural Engineering 2014;140:4013026. doi: 10.1061/(ASCE)ST.1943-541X.0000773.
[25] Su Y, Tian Y, Song X. Progressive Collapse resistance of Axially-Restrained Frame Beams. ACI Structural Journal 2009;106.
[26] Abaqus User Manual. Concrete Damage Plasticity, Abaqus Version 614.
[27] Popovics S. A numerical approach to the complete stress-strain curve of concrete. Cement and Concrete Research 1973;3:583–99.
[28] Belarbi A, Zhang L-X, Hsu TTC. Constitutive Laws of Reinforced Concrete Membrane Elements. Eleventh World Conference of Earthquake 1996:8.
[29] National Standard of People's Republic of China. Design Code for Reinforced Concrete Structures. 2002, Ministry of Housing and Urban-Rural Construction of the People's Republic of China and the General Administration of Quality Supervision, Inspection; Quarantine of the People's Republic of China.
[30] Dere Y, Koroglu MA. Nonlinear FE Modeling of Reinforced Concrete. International Journal of Structural and Civil Engineering Research J Struct Civ Eng Res 2017;6:71–4. doi:10.18178/ijscer.6.1.71-74.

Cite this Article: Sanjeev Bhatta, Jian Yang, Qing-Feng Liu. Finite Element Modeling of RC Beam Column Sub-assemblages Subjected to Column Loss Scenario. *International Journal of Structural Engineering and Analysis*. 2020; 6(2): 1–20p.